Journal of Power Sources 239 (2013) 103–110

Contents lists available at SciVerse ScienceDirect

Journal of Power Sources

journal homepage: www.elsevier.com/locate/jpowsour

Additive-free solvothermal synthesis and Li-ion intercalation properties of dumbbell-shaped $LiFePO_4$/C mesocrystals

Nan Zhou [a,b], Hai-Yan Wang [a], Evan Uchaker [b], Ming Zhang [b], Su-Qin Liu [a], You-Nian Liu [a,*], Guozhong Cao [b,**]

[a] College of Chemistry and Chemical Engineering, Central South University, Changsha, Hunan 410083, China
[b] Department of Materials Science and Engineering, University of Washington, Seattle, WA 98195, United States

HIGHLIGHTS

- Hierarchical dumbbell-shaped $LiFePO_4$ mesocrystals were fabricated without any additive.
- Co-solvent of DMF/EG was applied for the solvothermal synthesis of cathode materials.
- The DMF/EG co-solvent played a crucial role in the formation of dumbbell-shaped LFP mesocrystals.
- The formation of the LFP mesocrystals was possibly following a two-step process.
- The LFP/C mesocrystals show better storage performance at higher rate after in-situ carbon coated.

ARTICLE INFO

Article history:
Received 1 November 2012
Received in revised form
5 February 2013
Accepted 22 March 2013
Available online 2 April 2013

Keywords:
Mesocrystals
Lithium iron phosphate
Self-assembly
Lithium ion battery
Cathode
Nanorods

ABSTRACT

Hierarchical dumbbell-shaped lithium iron phosphate ($LiFePO_4$) mesocrystals were successfully fabricated via a simple one-step, rapid, additive-free solvothermal route. A mixture of dimethylformamide/ethylene glycol (DMF/EG) has been utilized as the co-solvent and found to play an important role in the formation of the hierarchical mesostructure. The obtained dumbbell-shaped mesocrystals consist of self-assembly $LiFePO_4$ nanorods each with 2–3 μm in length and 30–50 nm in diameter. Further temperature treatment was applied to increase the crystallinity of the $LiFePO_4$ mesocrystals. A high lithium ion intercalation capacity of 140 mA h g^{-1} was exhibited by the $LiFePO_4$ mesocrystal when tested under a discharge rate of 17 mA g^{-1}, which should be attributed to the fast intercalation reaction and easy mass and charge transfer offered by the large specific surface and short diffusion distance of dumbbell-shaped mesoporous composed of nano-sized $LiFePO_4$ rods. The nanorods can be carbon coated in-situ by adding sucrose during the solvothermal process and the $LiFePO_4$/C mesocrystals showed an improved electrochemical property at higher rates and good cyclic performance.

1. Introduction

Mesoscopically structured crystals (mesocrystals) are a new class of solid material superstructures constructed of crystallographically oriented nanocrystals and were first defined by Cölfen et al. [1] in 2005. These well-defined ensembles are composed of a few to thousands of hierarchically assembled nanoscaled primary unites and usually show different collective properties from those of individual nanoparticles as well as bulk materials with the same chemical composition [2]. These superstructures with new chemical and physical properties have been attracting interests and attentions from both chemical and physical fields. Mesocrystals were first found for biominerals and their mimetics [3–5], however, the high surface area and high porosity introduced by the superstructure, the well crystallized composition unites with small size, and easy process ability due to the micrometer size range of the whole architecture, all combined ensures the mesocrystals a new possibility for advanced materials design.

Lithium iron phosphate ($LiFePO_4$ or LFP hereafter) is one of the most promising cathode materials for the new generation of lithium ion battery due to the high theoretical capacity, flat discharge potential, abundant raw materials, environmentally benign, and excellent thermal and chemical stability [6]. However, the intrinsic low conductivity of $LiFePO_4$ around 10^{-11} S cm^{-1}

* Corresponding author. Tel.: +86 731 8883 6964; fax: +86 731 8887 9616.
** Corresponding author. Tel.: +1 206 616 9084; fax: +1 206 543 3100.
E-mail addresses: liuyounian@csu.edu.cn (Y.-N. Liu), gzcao@u.washington.edu (G. Cao).

0378-7753/$ – see front matter © 2013 Elsevier B.V. All rights reserved.
http://dx.doi.org/10.1016/j.jpowsour.2013.03.136

(compared with 10^{-3} S cm^{-1} for $LiCoO_2$ and 10^{-5} S cm^{-1} for $LiMn_2O_4$), largely hindered its widely commercialization as well as application in high energy and high power devices [7–9]. Decreasing the particle size, controlling morphology combined with carbon coating is considered to be the most effective way to address this problem [10], since increasing the specific surface area can accelerate the intercalation reaction and reduce the diffusion distance of lithium ions while appropriate conductive coating can strengthen the interface contact and improve the transfer of electrons. Thus, the study of novel hierarchical LFP self-assembly architectures has emerged and become a new topic of LFP study. A few micro-scale hierarchical assemblies with different shapes were successfully synthesized, characterized and reported [11–14]. However, expensive organic surfactants, complicate processes and long time reaction were required for those aforementioned works. The synthesis of novel self-assemble hierarchical LFP superstructures by sufficient routes still remains a challenge.

Solvothermal synthesis has been confirmed to be an efficient way to have phase purity, grain size and particle morphology controlled, where the solvent plays a crucial role [15,16]. N,N-dimethylformamide (DMF), a polar aprotic solvent with high-boiling point, is commonly used in metals [17,18], metal oxides [19,20], metal-organic frameworks [21,22], metal chalcogenides [23,24] synthesis with controlled shape and structures via solvothermal approach separately or cooperatively, taking advantages of easy operation, environmentally benign, and low-cost. Many hierarchical structures were obtained with the presence of DMF as solvent [25–27]. For example, urchin-like Ni-P microspheres constructed by thousands of nanoscale prominences resembling urchins were fabricated in water-DMF co-system by Ni et al. [27]. A high BET surface area of 425 m^2 g^{-1} was found for this urchin-like Ni-P architecture. Nanoflakes-built pyrite FeS_2 microspheres were synthesized through solvothermal method with a mixed solvent of DMF and ethylene glycol (EG) [28]. The composition of the mixed solvent and additive urea are crucial parameters for the formation of this uniform microsphere structure.

In this work, co-solvent system of DMF/EG was applied to synthesis hierarchical dumbbell-shaped $LiFePO_4$ mesocrystals via a simple one-step, rapid solvothermal route without any additives. To the authors' best knowledge, this is the first utilization of DMF as a solvent in the synthesis of cathode materials such as $LiFePO_4$ for lithium ion batteries. The effects of the mixed solvent on the formation of dumbbell LFP mesocrystals and the self-assembly mechanism were investigated. When sucrose was introduced to generate carbon coating, the self-assembled hierarchical dumbbell-shaped $LiFePO_4$-carbon mesocrystals showed improved storage property at high rates and good cyclic stability.

2. Experimental

2.1. Synthesis

Hierarchical dumbbell-shaped $LiFePO_4$ mesocrystals were synthesized via solvothermal method by using lithium dihydrogen phosphate LiH_2PO_4 (≥99.0%, Aesar) and Iron(II) oxalate dihydrate $FeC_2O_4 \cdot 2H_2O$ (≥99.0%, Aldrich) as precursors. A total of 0.8 mmol $FeC_2O_4 \cdot 2H_2O$ was first dissolved in 5 ml EG while stoichiometric amount of LiH_2PO_4 was dissolved in 5 ml DMF separately. Then the two solutions were mixed together and ultrasonicated for 1 h. The overall molar ratio of Li:Fe:P was 1:1:1. The obtained mixture was transferred into a 30 ml polytetrafluoroethylene (PTFE) inner steel autoclave and heated at 225 °C for 3.5 h. After that, the autoclave was taken out of the furnace and fast cooled to room temperature. The obtained product was washed with ethanol and de-ionized water for several times. To obtain in-situ carbon coated $LiFePO_4$/C mesocrystals, 0.2 mg sucrose was added and dissolved with LiH_2PO_4 in the DMF solvent before the mix and ultrasonicate treatment. The obtained pure and carbon coated $LiFePO_4$ mesocrystals were dried at 60 °C overnight followed with annealing in nitrogen gas environment for a dwell time of 5 h at 600 °C to guarantee better crystallinity and conductive coating. No other surfactants or template agents were added during the whole synthesis.

To investigate the influence of the DMF/EG co-solvent on the formation of hierarchical dumbbell-shaped $LiFePO_4$ mesocrystals, pure 10 ml EG and DMF were separately applied to the above mentioned precursors and following the same steps of the synthesis. For convenience, two sample notations are used in this paper: S_{EG} for pure EG solvent product and S_{DMF} for pure DMF solvent product.

The formation mechanism of hierarchical dumbbell-shaped $LiFePO_4$ mesocrystals was also investigated by changing the solvothermal synthesis duration time to 1 h, 2 h and 3 h with the same precursors, co-solvents and conditions of pure hierarchical dumbbell-shaped $LiFePO_4$ mesocrystals synthesis, except the heat treatment, noted as S_{1h}, S_{2h}, and S_{3h} later. The LFP mesocrystals without further calcination were also analyzed by XRD to determine the crystal phase after 3.5 h solvothermal reaction.

2.2. Structural characterization

Phase identification was taken by X-Ray Diffraction (XRD) employing a scan speed of 0.02° per second in the 2θ range from 10° to 60° using a D8 Bruker X-ray diffractometer equipped with Cu-Kα radiation. The accelerating voltage and current were 40 kV and 40 mA, respectively. Carbon content of the coated LFP/C sample was calculated based on thermogravimetric analysis (TGA) (Perkin–Elmer instruments) pattern carried out with the temperature range from room temperature to 700 °C under dry air flow at a heating rate of 5 °C/min. Morphology and size of all samples were taken by scanning electron microscopy (SEM) with a JEOL JSM-7000F field emission scanning electron microscope operated at 10 kV and 10 mA. Crystallinity, morphology as well as carbon coating thickness were measured by high-resolution transmission electron microscopy (HRTEM) images taken by a Tecnai G2 F20 transmission electron microscope with an acceleration voltage of 200 kV. Brunauer-Emmett-teller (BET) was utilized to examine the surface area of LFP and LFP/C mesocrystals.

2.3. Electrochemical measurements

For energy storage studies, the obtained pure LFP and LFP/C mesocrystals were mixed with super P carbon black and poly(vinyl difluoride) (PVDF) in the weight ratio 75:15:10 using N-methyl pyrrolidone (NMP) as solvent and then pasted on an aluminum foil to fabricate composite electrodes. The cathode films were assembled into R2016 coin-type cells in an Argon filled glove box. Lithium metal foil, 1 M $LiPF_6$ in ethylene carbonate (EC)/dimethyl carbonate (DMC) (1:1, in weight) and Celgard 2400 membrane were used as counter electrode, electrolyte and separator respectively. Charging-discharging cycling tests of the assembled cells at a constant current mode were carried out using a computer controlled electrochemical analyzer (Model BT2000, Arbin Instruments, USA) in the voltage range of 4.2–2.5 V. Electrochemical impedance spectroscopy (EIS) was performed with a Princeton electrochemical workstation (Parstat 2273). A sinusoidal excitation voltage of 5 mV with a frequency range from 0.01 Hz to 100 kHz was applied. All potentials cited in this paper are referred to Li/Li^+.

3. Results and discussion

Fig. 1 shows the morphology of the carbon coated (Fig. 1a, b) and uncoated (Fig. 1c, d) hierarchical dumbbell-shaped $LiFePO_4$ mesocrystals with different magnifications and angles of view. Uniformly sized dumbbell-shaped $LiFePO_4$ mesocrystals were successfully synthesized through solvothermal route using a DMF/EG co-solvent for 3.5 h, without any surfactant or additive. The obtained $LiFePO_4$ mesocrytals have a length of ~2–3 μm with a diameter of about 1.5 μm in the head and a diameter of about 300 nm in the middle. A close view of the mesocrystals reveals hierarchical morphology that composed of self-assembly primary $LiFePO_4$ nanoneedles and nanorods with a dipolar orientation (Fig. 1b). No obvious difference was found between the morphology of the carbon free or coated dumbbell-shaped $LiFePO_4$ mesocrystals, suggesting that the addition of sucrose has no detectable impact on the formation of the dumbbell structure. Fig. 1d shows that the primary $LiFePO_4$ units are nano-sized needles and rods, having a diameter of 30–50 nm. These nanorods grown branched and separated from each other, leaving abundant void space in the heads of the dumbbell, making the $LiFePO_4$ mesocrystals a highly porous structure with large surface area. The mesoporosity of the hierarchical dumbbell-shaped architectures was analyzed, and the LFP and LFP/C mesocrystals possess BET surface areas of 44.3 $m^2\ g^{-1}$ and 41.9 $m^2\ g^{-1}$, respectively.

Fig. 2 shows the XRD patterns of the pure and carbon coated hierarchical dumbbell-shaped $LiFePO_4$ mesocrystals. All intense peaks in both XRD patterns are indexed to an orthorhombic olivine space group (JCPDS card #040-1499), corresponding with crystallized $LiFePO_4$. No secondary phases such as FeP, $FePO_4$ or Li_3PO_4 and diffraction peaks of graphite were observed. Carbon derived from sucrose pyrolysis is likely to be amorphous and its presence has no detectable influence on the crystal structure of $LiFePO_4$.

Fig. 3 shows the TEM and HRTEM images of the carbon coated dumbbell-shaped $LiFePO_4$ mesocrystals. Fig. 3a (insert) illustrates a uniform dumbbell-shaped $LiFePO_4$ mesocrystal with lighter branch sides on the top and darker color of connected overlying rods on the middle part. High magnification images of the branched top (Fig. 3b, c) display the $LiFePO_4$ nanoneedles or nanorods of ~40 nm. The lighter layer around the architecture enlarged in HRTEM image Fig. 3d depicts the carbon coating resulted from pyrolysis of sucrose. However, the layer of carbon coating is not so homogeneous and has an average thickness of approximate 1.5 nm. Since each mesocrystal is an assembly of a large number of small needles or nanorods, and carbon and $LiFePO_4$ are very different in their surface properties, the uniform carbon coating on every individual needle or rod is difficult. The lattice fringes in Fig. 3f value

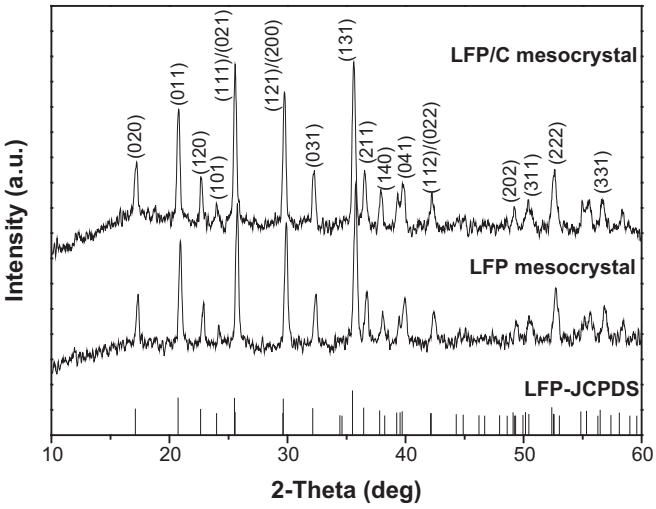

Fig. 2. X-Ray diffraction patterns of the LFP and LFP/C mesocrystals heated at 600 °C for 5 h, and LFP-JCPDS.

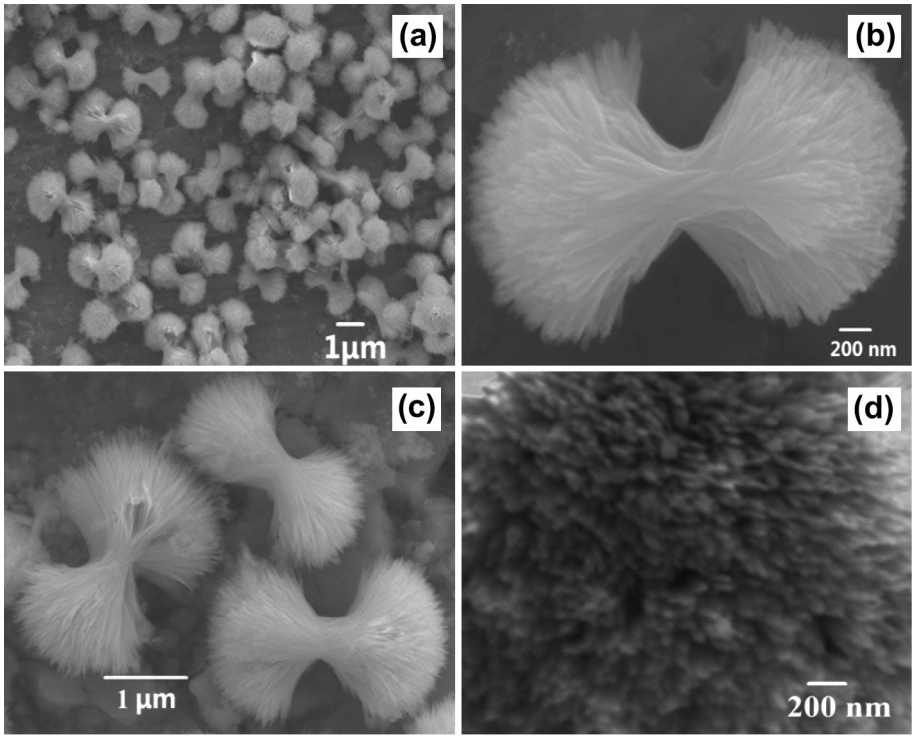

Fig. 1. SEM images of carbon coated (a, b) and pure (c, d) hierarchical dumbbell-shaped $LiFePO_4$ mesocrystals.

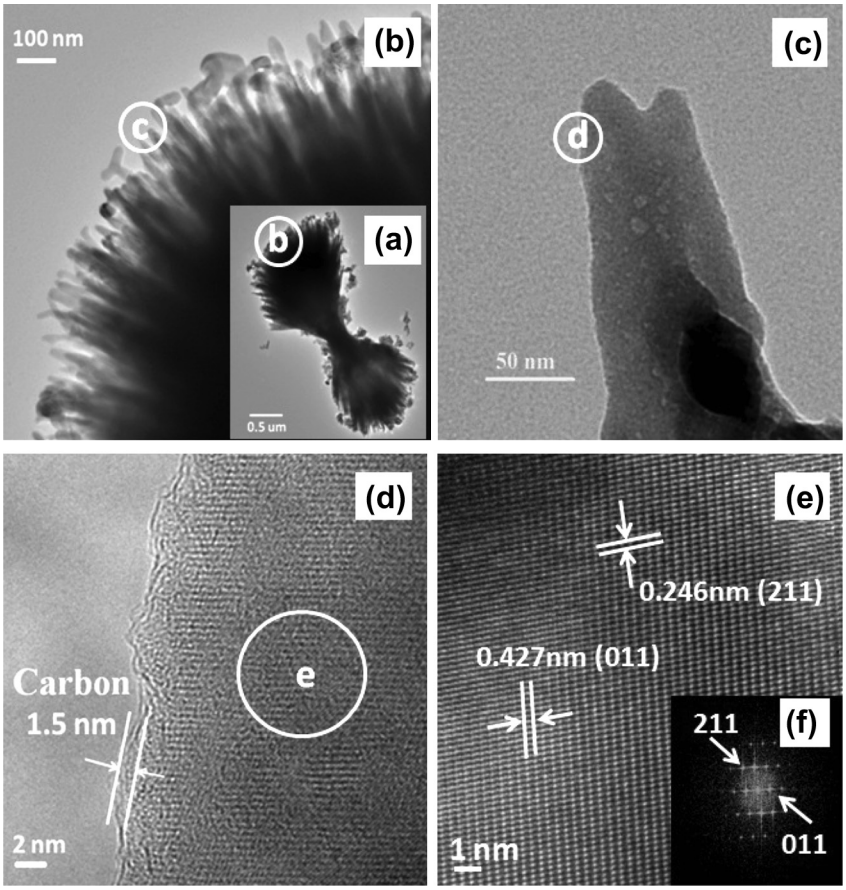

Fig. 3. TEM image (insert (a)) (b, c), HRTEM image (d, e) and corresponding Fast Fourier Transform pattern (insert (f)) of carbon coated hierarchical dumbbell-shaped $LiFePO_4$ mesocrystals.

d-spacing of 0.427 nm and 0.246 nm correspond to the (011) and (211) planes of the orthorhombic phase $LiFePO_4$. In addition, the corresponding Fast Fourier Transform (FFT) analysis shown in the insert of Fig. 3f depicts a single crystalline pattern with sharp diffraction dots, further confirms the primary units of the dumbbell-shaped $LiFePO_4$ mesocrystals are well crystallized olivine LFP material.

To investigate the effect of DMF/EG co-solvent on the formation of hierarchical dumbbell-shaped $LiFePO_4$ mesocrystals, pure 10 ml respective EG and DMF solvent were used in the solvothermal process with all other parameters kept unchanged. Figs. 4 and 5 show the morphology and crystal phases of the products obtained from these two pure solvents under the same synthesis condition respectively. For sample S_{EG}, platelet-shaped particles were found in the SEM images (Fig. 4a), combined with a large fraction of cuboids. The XRD pattern of this sample showed weak peaks corresponding to orthorhombic $LiFePO_4$. But a strong peak indexed to Li_3PO_4 as well as several small peaks possibly belong to Li_3PO_4, Fe_3PO_4, Fe_2O_3 and other unknown crystals were also detected. It is reported that Li_3PO_4 likely to be a transition phase before the formation of $LiFePO_4$ [11] and platelet-shaped $LiFePO_4$ particles could be obtained by using EG as solvent through solvothermal synthesis [16,29]. The few platelet particles morphology and weak peaks of olivine LFP crystal pattern found in this sample suggested that the reactions in the $LiFePO_4$ synthesis could not be finished in such a short time by using the pure solvent EG. The sample synthesized with pure DMF solvent consisted of small irregular spheres (Fig. 4b). The XRD pattern of this sample showed only one weak peak corresponding to olivine $LiFePO_4$, but strong peak of Li_3PO_4 as well as some small peaks corresponding to Li_3PO_4, Fe_3PO_4, Fe_2O_3 and unknown crystals (Fig. 5). Again, since Li_3PO_4 is considered to be a transition phase before the formation of $LiFePO_4$ [11], it could be assumed that $LiFePO_4$ might be synthesized in pure DMF solvent when a long reaction time is used.

No single uniform hierarchical dumbbell-shaped $LiFePO_4$ architecture was detected in either of these two samples, indicating the indispensable role of the DMF/EG co-solvent in the formation of dumbbell $LiFePO_4$ mesocrystals. The formation of the unique dumbbell-shaped $LiFePO_4$ mesocrystals should be attributed to the presence of both EG and DMF in the system. Though the exact mechanism or the roles that EG and DMF played are not known, they may have provided required interface energy, chemistry, and ion diffusivity for $LiFePO_4$ crystal to grow and to assemble to the dumbbell-shaped mesocrystals. The reaction condition and obtained products of the LFP and LFP/C mesocrystals, S_{EG} and S_{DMF} were summarized in Table 1. Hierarchical dumbbell-shaped $LiFePO_4$ mesocrystals can only be synthesized from the mixed DMF/EG solvent and well crystallized pure and carbon coated olivine LFP material can be obtained after heat treatment.

To study the assembly mechanism of the dumbbell-shaped $LiFePO_4$ mesocrystals, solvothermal synthesis with different reaction time of 1 h, 2 h and 3 h were carried out, with other conditions kept the same. The crystal phases of the obtained products were investigated by XRD, with the results shown in Fig. 6. Both XRD patterns of sample S_{1h} and S_{2h} demonstrated an intense peak of Li_3PO_4 and some weak peaks, suggesting the initial formation of Li_3PO_4 at the beginning of the reaction. Fe^{3+} containing chemicals including FeP, Fe_3O_4, and Fe_3PO_7 were also detected in these two

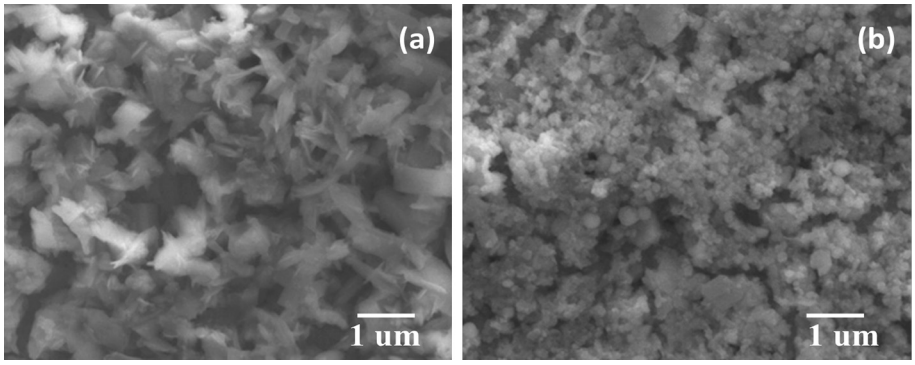

Fig. 4. SEM images of sample S_{EG} (a) and S_{DMF} (b).

samples, possibly formed during the cooling process, as the formation reaction of Li_3PO_4 seems not complete within 2 h. More peaks belonging to Li_3PO_4 phase were found in sample S_{2h} than in sample S_{1h}, demonstrating the phase transition to Li_3PO_4 during the reaction. After 3 h solvothermal synthesis, diffraction peaks for $LiFePO_4$ were emerged while the sharp peak of Li_3PO_4 as well as other peaks of impurity phases disappeared, indicating the phase transformation of Li_3PO_4 to $LiFePO_4$ started. Pure crystal phase of LFP mesocrystals was obtained after 3.5 h solvothermal synthesis, confirming the phase transformation of the formation process of hierarchical dumbbell-shaped $LiFePO_4$ architectures, which corroborates well with the conclusion in literature [11]. However, the peaks corresponding to orthorhombic olivine LFP were so weak, suggesting poor crystallinity of $LiFePO_4$ mesocrystals, which could be enhanced by further heat treatment at 600 °C for 5 h.

Fig. 7 displays the SEM images of product obtained at different reaction time. For sample S_{1h} (Fig. 7a), most of the product remained nano-sized particles, indicating that $LiFePO_4$ growth was not finished in such a short duration. After 2 h reaction, nanorods were obtained and began to assemble to dumbbell-shaped architectures, as shown in Fig. 7b. The interesting thing is those nanorods or needles were somehow aligned in parallel in certain crystal orientation rather than aggregated together, which normally happens in nano-sized materials to decrease the surface energy [30–32]. This situation could possibly be a result of the cooperation of DMF/EG co-solvents, due to which interface energy, chemistry or ion diffusivity might have been applied during the formation process. Numbers of dumbbell-shaped $LiFePO_4$ structures appeared after 3 h solvothermal synthesis (Fig. 7c) with different size, demonstrating the incomplete of the self-assembly.

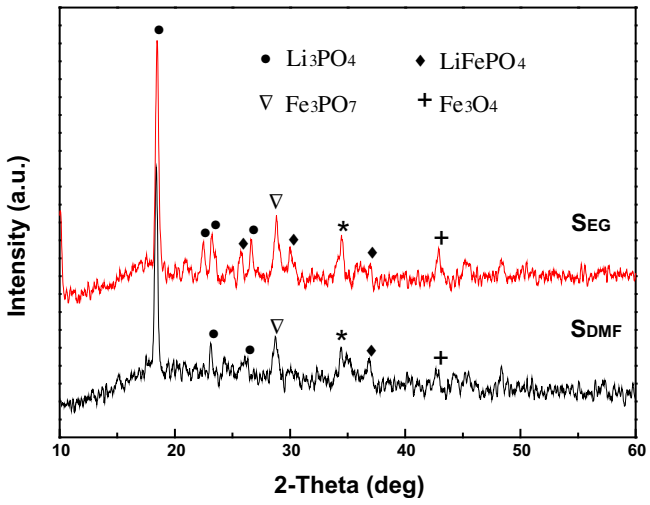

Fig. 5. XRD patterns of sample S_{EG} and S_{DMF}.

The experimental results strongly suggest the formation of $LiFePO_4$ mesocrystals took a two step process, as schematically illustrated in Fig. 7d: formation of Li_3PO_4 crystals first and then phase transformation from Li_3PO_4 crystals to $LiFePO_4$ crystals, which agrees with the literatures [11,33]. It should be noted that in the literature, different opinions exist about the mechanism for the LFP dumbbell formation. For example, some attributed the formation of dumbbell shape LFP nanodendrites to the Van der Walls attraction as a result of hydrophobic interaction due to the bonded surfactant molecules at the end of the nanorods [33]. Others concluded that the dumbbell-shaped LFP architectures were recrystallized from the 3D structured aggregates under lattice tension or surface interaction at the edge areas [11]. It was suggested that special surfactants played a crucial role in the solvothermal synthesis of dumbbell LFP architectures in both reports. Our experiments revealed that no surfactant or additives was necessary for the fabrication of hierarchical $LiFePO_4$ dumbbell-shaped mesocrystals, though the formation of this structure required the use of mixed DMF/EG solvent.

The obtained pure LFP and LFP/C mesocrystals were mixed with carbon black and PVDF binder to fabricate composite electrodes and assembled into coin cells to characterize the electrochemical properties. The carbon content of the LFP/C sample was calculated according to TGA result and turned out to be 2.2 wt%. The mass of carbon was not included when calculating the specific capacity of the LFP/C mesocrystals since the capacity of the nanocarbon coating was negligible in the voltage range of 2.5 V to 4.2 V. Three cycles of lithium ion charge–discharge process at a current density of 17 mA g^{-1} (0.1 C) in the hierarchical dumbbell-shaped $LiFePO_4$ mesocrystals and its carbon coated counterpart structures were displayed in Fig. 8. The pure hierarchical dumbbell-shaped $LiFePO_4$ mesocrystals exhibited an initial charge capacity of about 110 mA h g^{-1}, with a voltage plateau at ~3.5 V. This mesocrystals showed a higher lithium ion intercalation storage property of

Table 1
Effect of solvents on particle morphology and crystals structure of the sample.

Sample	DMF/EG (ml)	T/t (°C/h)	Sucrose (mg)	Crystalline phases	Particle morphology
LFP	5/5	225/3.5	0	$LiFePO_4$	Dumbbell-shape structure
LFP/C	5/5	225/3.5	0.2	$LiFePO_4$	Dumbbell-shape structure
S_{EG}	10/0	225/3.5	0	Multi-phases	Plates + cuboids
S_{DMF}	0/10	225/3.5	0	Multi-phases	Spheres + cuboids

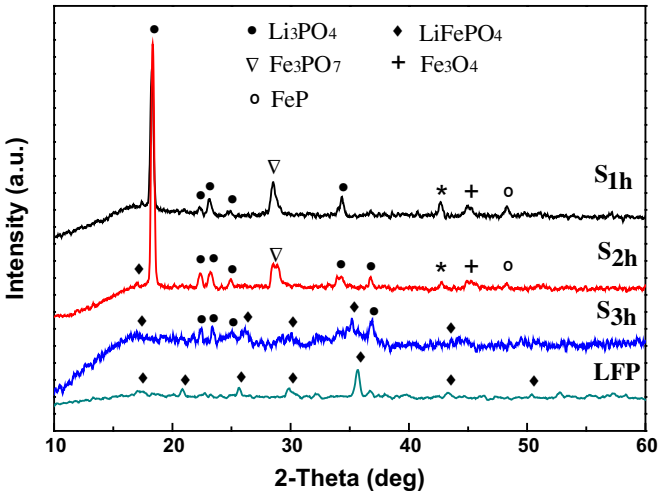

Fig. 6. XRD patterns of samples derived from different reaction time.

140 mA h g^{-1} with voltage plateau at ~3.35 V (Fig. 8a). The polarization between the charge and discharge plateaus was quickly reduced from the second cycle and became steady, revealed the penetration of electrolyte after the first charging process and the formation of an active surface layer of $LiFePO_4$ [34]. The hierarchical dumbbell-shaped $LiFePO_4$ mesocrystals with nanocarbon coating showed higher initial charge capability of 125 mA h g^{-1} but almost the same lithium intercalation capacity of 143 mA h g^{-1} at the same rate of 0.1 C (Fig. 8b). This storage capability of carbon coated hierarchical dumbbell-shaped $LiFePO_4$ mesocrystals could not reach the theoretical value (170 mAh g^{-1}) as compared to other nano-sized LFP structures, possibly attributable to the inhomogeneous and/or incomplete carbon coating. However, lower lithium storage capability was reported for other LFP mesocrystals and the author contribute to the low electronic conductivity and slow lithium ion diffusion [14]. The hierarchical dumbbell-shaped $LiFePO_4$ mesocrystals are highly porous with large specific surface area, nano-sized primary crystals with much shortened diffusion path of lithium ions would definitely result in improved electrochemical intercalation properties. The polarization between the charge and discharge curves of the carbon coated $LiFePO_4$ mesocrystals was also reduced and became steady when the number of cycles increased, with an improved charge plateau at about 3.46 V and discharge plateau at about 3.4 V. Besides, the hysteresis (the difference between the anodic and cathodic peak voltages) of the carbon coated hierarchical dumbbell-shaped $LiFePO_4$ mesocrystal architectures showed much lower value than that of carbon free ones, indicating faster insertion and extraction of lithium ions with carbon coating.

The flat plateaus during the charge–discharge process for both LFP and LFP/C mesocrystals correspond well with the typical two-phase reactions of lithium insertion and extraction between olivine $LiFePO_4$ and $FePO_4$. However, shorter plateau and longer sloping region was found in the charge and discharge curves of the LFP and C-coated mesocrystals when compared with conventional $LiFePO_4$ materials. Similar phenomenon has also been detected in other hierarchical $LiFePO_4$ mesostructures and two possible explanations were given out [11,12]. One is the formation of a single-phase solid solution found in nanostructures with particle size under 45 nm [35,36]. The other is contributing the slope to the capacitive behavior of the surface or interfacial storage of lithium ions, which has been termed the pseudo-capacitive effect and has been found in materials with high surface area and nanostructures [37–40]. Although the composition units are nano-sized LFP rods with a diameter around 40 nm, the length of these nanorods are more than 1 μm and the whole $LiFePO_4$ mesocrystals hold a micro-sized structure, both of which are much larger than the critical size to form a solid solution. The total storage capacitance of the LFP mesocrystals should be attributed to both lithium ion intercalation and surface capacitive adsorption [41].

Another thing needs to mention is that the initial Coulombic efficiency (calculated from discharge capacity/charge capacity) is greater than 100% for both pure and carbon coated hierarchical $LiFePO_4$ mesocrystals, suggesting more Li^+ intercalated into the mesocrystal while less Li^+ deintercalated. The unusual initial Coulombic efficiency could be result from the initial deficient amount of Li ions in the mesocrystals after short reaction duration of 3.5 h through solvothermal synthesis, in spite of a stoichiometric ratio of the precursors were used in this work.

Fig. 9 shows the rate capability of both LFP and LFP/C mesocrystals characterized under varied current densities for every five

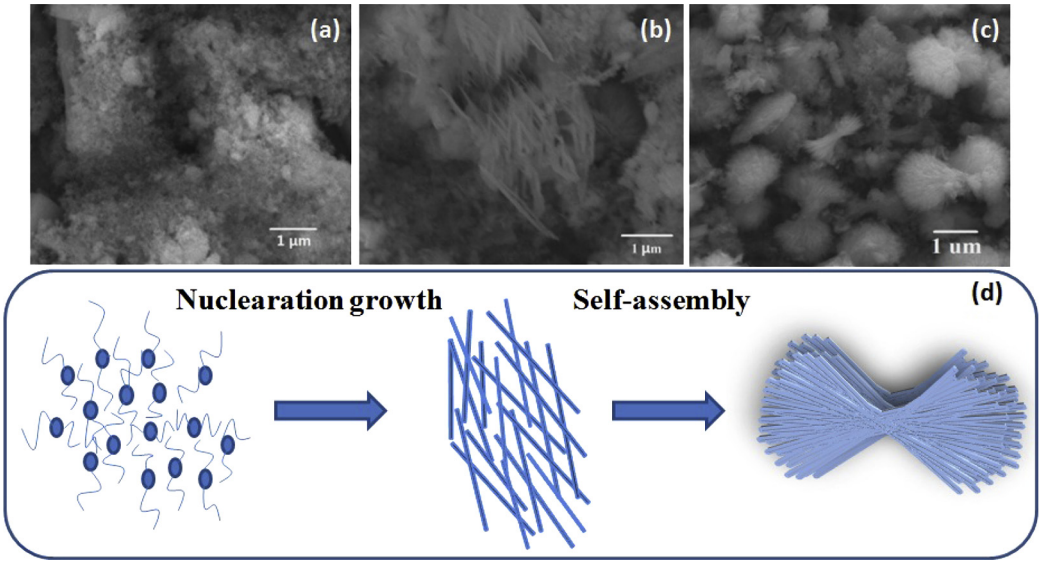

Fig. 7. SEM images of samples (a) S_{1h}, (b) S_{2h}, (c) LFP mesocrystals and schematic illustration of the formation of hierarchical dumbbell-shaped $LiFePO_4$ mesocrystals.

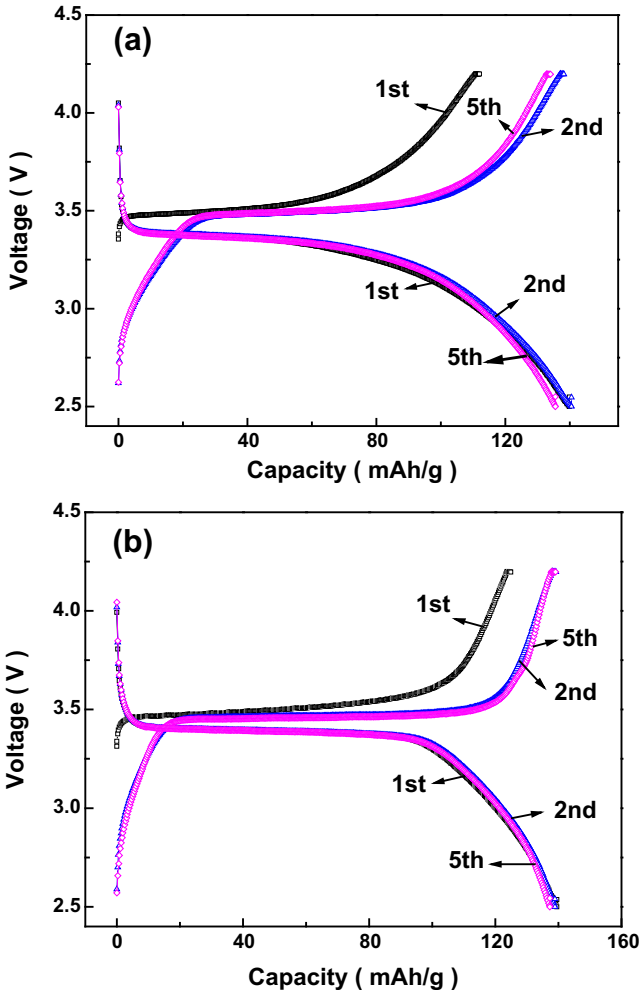

Fig. 8. Three cycles of lithium ion charge–discharge process of LFP mesocrystals (a) and LFP/C mesocrystals (b) at 0.1 C rate between 2.5 and 4.2 V.

cycles. Gradual decrease of discharge capacity with increase rate found for both samples is commonly the case for electrodes. For different rates of 0.2 C, 0.5 C, 1 C and 5 C, the LFP/C mesocrystals exhibited high lithium storage property of 131 mA h g^{-1}, 120 mA h g^{-1}, 109 mA h g^{-1}, and 84 mA h g^{-1}, while the LFP mesocrystals only displayed 119 mA h g^{-1}, 97 mA h g^{-1}, 73 mA h g^{-1} and 38 mA h g^{-1} under the same test condition, respectively. Especially when the rate increased as high as 10 C, the discharge capacity of LFP mesocrystals only remained 5 mA h g^{-1}, while a 68 mA h g^{-1} capability was still obtained for LFP/C mesocrystals. Although the nanocarbon was not uniformly coated on the whole surface of single needle or rod of the hierarchical dumbbell-shaped $LiFePO_4$ mesocrystal structures, the electrochemical property of the $LiFePO_4$/C mesocrystals was still greatly improved by the introduction of conductive carbon, especially at higher rates.

Fig. 10 shows the long-term cyclic performance of the carbon coated hierarchical dumbbell-shaped $LiFePO_4$ mesocrystals at rate of 0.5 C and the Coulombic efficiency. The discharge capacity of this electrode dropped 8.7% at the 0.5 C rate after 70 cycles and the Coulombic efficiency maintained above 95% for all the charge and discharge processes. This cyclic stability of the $LiFePO_4$/C mesocrystals is not outstanding when compared to other nano-sized C-LFP materials [15], which should possibly be contributed to the inhomogeneous and incomplete carbon coating.

EIS tests were carried out to analyze the inner impedance of pure and carbon coated LFP mesocrystal electrodes. Before EIS tests, all the cells were subjected to charge and discharge for two cycles to guarantee the penetration of electrolyte and formation of active layer. Fig. 11 represents the Nyquist plots of LFP and LFP/C mesocrystals tested at open circuit under ambient temperature. Both EIS spectra curves of pure LFP and carbon coated LFP mesocrystals show a semicircle in high frequency region and a slop line in low frequency region. An equivalent circuit (inset of Fig. 11) was employed to explain the obtained EIS spectra: where R_s represents the resistance of electrolyte, R_{ct} relates to the charge transfer resistance, CPE refers to the constant phase element (CPE) corresponded to R_{ct}, and Z_w is the Warburg impedance associated with the diffusion of Li ions into bulk materials. The charge transfer resistance of pure and carbon coated $LiFePO_4$ mesocrystals were 316 Ω and 286 Ω, respectively, suggesting faster charge transfer between the electrolyte and the $LiFePO_4$ material in LFP/C mesocrystals, which confirms the electronic conductivity of LFP mesocrystals could be enhanced by nanocarbon coating. This corroborates well with the results of charge–discharge profiles.

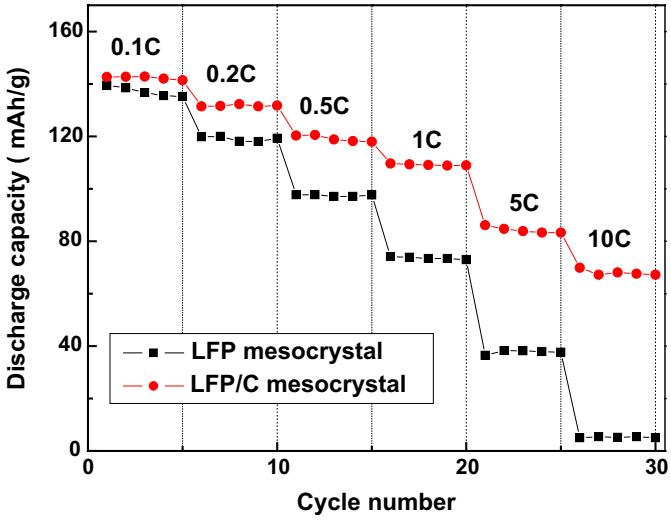

Fig. 9. Energy storage performance of the LFP and LFP/C mesocrystals at different rates between 2.5 and 4.2 V.

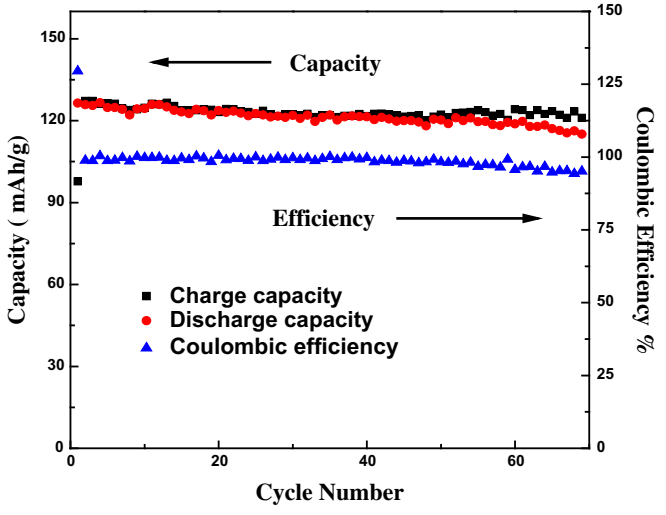

Fig. 10. Cyclic performance and Coulombic efficiency of the LFP/C mesocrystals at 0.5 C rate between 2.5 and 4.2 V.

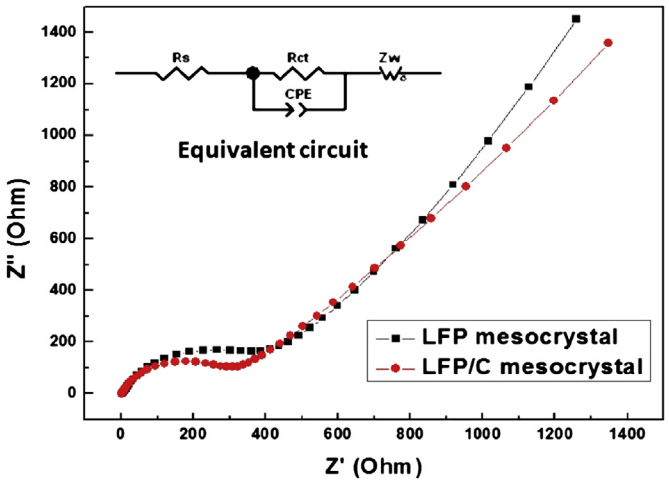

Fig. 11. Nyquist plots of LFP and LFP/C mesocrystals. Inset is the equivalent circuit.

4. Conclusions

Hierarchical dumbbell-shaped $LiFePO_4$ mesocrystals were successfully fabricated via solvothermal route without any additive. A mixture of DMF/EG was utilized as co-solvent for the synthesis reaction and played a crucial role in the formation of the hierarchical mesostructures. The obtained dumbbell-shaped LFP mesocrystals were constructed of well crystallized $LiFePO_4$ nanoneedles or nanorods with 30–50 nm in diameter by self-assembly. The highly porous mesocrystals were micro-sized architectures with 2–3 μm in length and 300 nm diameter. Both the pure and carbon coated $LiFePO_4$ mesocrystals were annealed at 600 °C for 5 h to increase the crystallinity. High lithium intercalation capacity of 140 mA h g^{-1} and 143 mA h g^{-1} were exhibited by pure and carbon coated $LiFePO_4$ mesocrystal at 0.1 C rate, respectively. This good electrochemical performance was attributed to the fast intercalation reaction and easy electron transport offered by the large specific surface area of dumbbell-shaped mesoporous structure. The nanoneedles and rods can be in-situ carbon coated by adding sucrose during the solvothermal process and the $LiFePO_4$/C mesocrystals showed greatly improved lithium storage property at higher rates and good cyclic performance.

Acknowledgement

NZ gratefully acknowledges fellowship from the China Scholarship Council. This research work has been financially supported in part by the National Science Foundation (NSF (gs1), CMMI-1030048) and the University of Washington TGIF grant.

References

[1] H. Colfen, M. Antonietti, Angewandte Chemie-International Edition 44 (2005) 5576–5591.
[2] J. Fang, B. Ding, H. Gleiter, Chemical Society Reviews 40 (2011) 5347–5360.
[3] R.-Q. Song, H. Coelfen, Advanced Materials 22 (2010) 1301–1330.
[4] A.W. Xu, M. Antonietti, H. Colfen, Y.P. Fang, Advanced Functional Materials 16 (2006) 903–908.
[5] A.N. Kulak, P. Iddon, Y. Li, S.P. Armes, H. Cölfen, O. Paris, et al., Journal of the American Chemical Society 129 (2007) 3729–3736.
[6] A.S. Andersson, J.O. Thomas, B. Kalska, L. Haggstrom, Electrochemical and Solid State Letters 3 (2000) 66–68.
[7] C. Delacourt, L. Laffont, R. Bouchet, C. Wurm, J.B. Leriche, M. Morcrette, et al., Journal of the Electrochemical Society 152 (2005) A913–A921.
[8] W. Ojczyk, J. Marzec, K. Swierczek, W. Zajac, M. Molenda, R. Dziembaj, et al., Journal of Power Sources 173 (2007) 700–706.
[9] D. Morgan, A. Van der Ven, G. Ceder, Electrochemical and Solid State Letters 7 (2004) A30–A32.
[10] J. Wang, X. Sun, Energy & Environmental Science 5 (2012) 5163–5185.
[11] H. Yang, X.L. Wu, M.H. Cao, Y.G. Guo, Journal of Physical Chemistry C 113 (2009) 3345–3351.
[12] D. Rangappa, K. Sone, T. Kudo, I. Honma, Journal of Power Sources 195 (2010) 6167–6171.
[13] H. Uchiyama, H. Imai, Crystal Growth & Design 10 (2010) 1777–1781.
[14] J. Popovic, R. Demir-Cakan, J. Tornow, M. Morcrette, D.S. Su, R. Schloegl, et al., Small 7 (2011) 1127–1135.
[15] S. Yang, X. Zhou, J. Zhang, Z. Liu, Journal of Materials Chemistry 20 (2010) 8086–8091.
[16] K. Saravanan, P. Balaya, M.V. Reddy, B.V.R. Chowdari, J.J. Vittal, Energy & Environmental Science 3 (2010) 457–464.
[17] X.L. Meng, S.M. Zhang, H. Xu, K.Z. Liu, Z.S. Wu, Z.J. Zhang, Zeitschrift Fur Naturforschung Section B – A Journal of Chemical Sciences 64 (2009) 929–934.
[18] Q. Lu, K.J. Lee, K.B. Lee, H.T. Kim, J. Lee, N.V. Myung, et al., Journal of Colloid and Interface Science 342 (2010) 8–17.
[19] Y. Chang, J.J. Teo, H.C. Zeng, Langmuir 21 (2005) 1074–1079.
[20] S.L. Xu, S.X. Sun, G.Z. Chen, T. You, X.Y. Song, Crystal Research and Technology 44 (2009) 721–724.
[21] W. Xu, Y. Wang, X. Bai, B.A. Dong, Q.O. Liu, J.S. Chen, et al., Journal of Physical Chemistry C 114 (2010) 14,018–14,024.
[22] K.H. Cui, S.Y. Yao, H.Q. Li, Y.T. Li, H.P. Zhao, C.J. Jiang, et al., Crystengcomm 13 (2011) 3432–3437.
[23] Q.F. Han, M.J. Wang, J.W. Zhu, X.D. Wu, L.D. Lu, X. Wang, Journal of Alloys and Compounds 509 (2011) 2180–2185.
[24] Q.F. Han, F. Qiang, M.J. Wang, J.W. Zhu, L.D. Lu, X. Wang, Materials Research Bulletin 45 (2010) 813–817.
[25] Y.H. Ni, L.N. Jin, L. Zhang, J.M. Hong, Journal of Materials Chemistry 20 (2010) 6430–6436.
[26] L. Jin, J. Hong, Y. Ni, Materials Chemistry and Physics 123 (2010) 337–342.
[27] Y. Ni, K. Mi, C. Cheng, J. Xia, X. Ma, J. Hong, Chemical Communications 47 (2011) 5891–5893.
[28] D. Wang, M. Wu, Q. Wang, T. Wang, J. Chen, Ionics 17 (2011) 163–167.
[29] K. Saravanan, M.V. Reddy, P. Balaya, H. Gong, B.V.R. Chowdari, J.J. Vittal, Journal of Materials Chemistry 19 (2009) 605–610.
[30] T.P. Chou, Q. Zhang, G.E. Fryxell, G. Cao, Advanced Materials 19 (2007) 2588–2592.
[31] Q. Zhang, G. Cao, Journal of Materials Chemistry 21 (2011) 6769–6774.
[32] M.M. Khin, A.S. Nair, V.J. Babu, R. Murugan, S. Ramakrishna, Energy & Environmental Sciences 5 (2012) 8075–8109.
[33] F. Teng, S. Santhanagopalan, A. Asthana, X. Geng, S.-I. Mho, R. Shahbazian-Yassar, et al., Journal of Crystal Growth 312 (2010) 3493–3502.
[34] X.L. Wu, L.Y. Jiang, F.F. Cao, Y.G. Guo, L.J. Wan, Advanced Materials 21 (2009) 2710–2714.
[35] N. Meethong, H.Y.S. Huang, W.C. Carter, Y.M. Chiang, Electrochemical and Solid State Letters 10 (2007) A134–A138.
[36] P. Gibot, M. Casas-Cabanas, L. Laffont, S. Levasseur, P. Carlach, S. Hamelet, et al., Nature Materials 7 (2008) 741–747.
[37] J. Wang, J. Polleux, J. Lim, B. Dunn, Journal of Physical Chemistry C 111 (2007) 14,925–14,931.
[38] H. Zhang, G.R. Li, L.P. An, T.Y. Yan, X.P. Gao, H.Y. Zhu, Journal of Physical Chemistry C 111 (2007) 6143–6148.
[39] J.Y. Luo, Y.G. Wang, H.M. Xiong, Y.Y. Xia, Chemistry of Materials 19 (2007) 4791–4795.
[40] J. Maier, Nature Materials 4 (2005) 805–815.
[41] M. Winter, R.J. Brodd, Chemical Reviews 105 (2005) 1021.